

New Approach to Rayleigh Guide Beacons

M. Lloyd-Hart, S. M. Jefferies, E. K. Hege, and J. R. P. Angel

Center for Astronomical Adaptive Optics, University of Arizona, Tucson, AZ 85721

<http://athene.as.arizona.edu:8000/caao>

Presented at SPIE conference number 4007 on
Adaptive Optical Systems Technology
Munich, March 31, 2000

New Approach to Rayleigh Guide Beacons

M. Lloyd-Hart, S. M. Jefferies, E. K. Hege, and J. R. P. Angel

Center for Astronomical Adaptive Optics, University of Arizona, Tucson, AZ 85721

ABSTRACT

We present analysis and numerical simulations of a new method to sense atmospheric wavefront distortion in real time with Rayleigh beacons. Multiple range-gated images of a single pulse from the laser are used to determine each phase map, providing an advantage over other methods in that photon noise is substantially reduced for a given brightness of the beacon. A laser at about 350 nm projects collimated pulses of light adjacent to the telescope. Rayleigh-scattered light from each pulse is recorded through the full telescope aperture in a sequence of video frames, each a few μs long. Images are captured as the pulse approaches and passes through the height at which the camera is focused. Phase diversity is thus naturally introduced between the frames. An iterative algorithm is used to extract the pupil-plane phases from the recorded intensity distributions.

We anticipate that such beacons are likely to be valuable in future advanced systems for adaptive optics on very large telescopes with multiple laser beacons and deformable mirrors that aim to provide a large corrected field of view by tomography of the atmospheric turbulence.

1. INTRODUCTION

Most groups now implementing adaptive optics on the world's large telescopes, including our own at Steward Observatory, are planning to use a laser guide star created by resonance scattering in the high mesospheric sodium layer. Our own group has made extensive tests of different sodium lasers at the old 6-mirror MMT. We showed that narrow band CW lasers give the highest efficiency excitation of the sodium layer, measuring the return explicitly as a function of column density.¹ A developmental sodium laser will be installed next spring at the newly refurbished 6.5 m MMT with adaptive secondary mirror.

There remain, however, considerable technical challenges which have not yet been overcome to make any practical, everyday laser system. Foremost is the need for a robust, reliable laser capable of exciting a bright, sharp beacon. Efficient excitation of the sodium resonance is critically dependent on pulse format, average power, tuning and bandwidth. Even if a good, robust laser meeting the requirements becomes available, there will still remain deficiencies with any single-laser system. Correction will be possible only over a small field of view, and even for on-axis imaging the finite height of the sodium beacon will result in a fundamental error in wavefront measurement, due to the cone effect or focus anisoplanatism.

Both limitations can be overcome if multiple guide stars are used. By measuring the wavefronts of several laser beacons in and around the cylinder swept out by starlight striking the primary mirror, the vertical structure of turbulence can be deduced. The uncertainty in the height of turbulence which is the origin of the cone effect is reduced or removed. Even the large cone effect of a Rayleigh beacon, which may be only twice the height of higher turbulent layers, no longer severely compromises or rules out their use. Further, if correction is done with two or more deformable mirrors at different well-chosen conjugates, the field of view is increased.

The possibility of using Rayleigh beacons in multiple laser systems has encouraged us to rethink their use for adaptive optics. They have fundamental practical advantages: there are no tuning or bandwidth requirements and lasers well suited to the task that are well engineered, robust and powerful are already made commercially.

We propose a new method to sense atmospheric wavefront distortion with Rayleigh beacons. In this new approach, a near diffraction-limited laser emitting UV pulses of < 100 ns is used to project columns of light instantaneously < 30 m long and < 10 cm wide at high altitudes. A "movie" of the rising narrow column can be recorded through the full telescope aperture, with some dozen sequential frames each on the order of a microsecond long.

Wavefront sensors used with Rayleigh beacons are normally limited to a single range-gated exposure of a few microseconds to prevent blurring. (An 8 m telescope focused at ~ 20 km height has a depth of field for seeing limited images of only 150 m or

1 μ s). In our case, since the narrow-beam source itself remains sharp, structure appearing in defocused images seen back at the telescope will reflect the atmospheric turbulence in the returning beam. The wavefront aberration will be computed using a phase diversity algorithm, the same approach used to determine the aberration of the Hubble Telescope from defocused images. The reduction will be performed in real time for closed-loop adaptive correction.

The advantage of this approach is reduced photon noise, because a much larger fraction of the Rayleigh scattered light is recorded. In the application to extremely large telescopes, where a dozen or more beacons might be needed to eliminate the cone effect and obtain atmospheric tomography, the added efficiency could be translated into an order of magnitude reduction in the number of lasers required to obtain the integrated flux by using each laser to feed multiple beacon projectors. Such efficiency could bring multiple-beam tomographic systems much closer to reality.

2. MEASURING THE WAVEFRONT WITH A PHASE-DIVERSE LASER BEACON

When light falls on a detector, only the squared amplitude of the electric vector is recorded; all information about the phase is lost. Wavefront sensors therefore rely on various schemes to encode phase information in the measured intensity. It has been known for years that the phase in the pupil plane of an optical system can in principle be recovered unambiguously from a pair of images recorded near the focal plane, with a small known defocus deliberately introduced between the two.^{2,3}

If two or more images of a reference beacon can be recorded and analyzed sufficiently rapidly and with adequate signal-to-noise, this technique can be used as a real-time wavefront sensor in an AO system. The method was first put to the test by us in 1990 to phase two of the six mirrors of the Multiple Mirror Telescope in real time.⁴ Tip, tilt and piston for each mirror were derived by an artificial neural network on the basis of two focal plane images of a star recorded simultaneously on the same detector, with a known focal shift between the two. In related experiments, the diffraction limit of the six-mirror array was recovered by correcting phase errors between five of the array elements on the basis of the measured interference pattern in the focal plane.⁵ The algorithm implemented a real-time Fourier transform in a manner similar to the algorithm for phase diversity.

When a pulsed laser rather than a star is used to generate a beacon, propagation of the laser pulse provides a very natural way to obtain multiple images at different focal positions (figure 1). In this example, a laser pulse is transmitted along the telescope's axis. A fast video camera focused at some nominal altitude views the pulse as it rises, through the full aperture of the telescope. Figure 2 shows a simulated sequence of frames that might be recorded by the camera as the laser pulse approaches and passes through focus.

3. IMPROVEMENT IN SIGNAL-TO-NOISE RATIO

As light from the laser rises through the atmosphere, Rayleigh scattering sends a continuous stream of light back to the telescope. AO systems which rely on this approach to generate an artificial guide star must therefore use a pulsed laser with a range-gated WFS detector to capture only those photons scattered from a selected height above the telescope. The typical setup, for instance the 3.5 m telescope at the Starfire Optical Range,⁶ uses a Shack-Hartmann WFS whose range gate is open for only a few microseconds. A longer exposure would result in smearing of the beacon image seen by the individual WFS subapertures because of parallax, which would degrade the sensitivity of the sensor, and overall system performance.

In contrast, the new approach takes advantage of the natural defocusing of the beacon image. Individual exposures are subject to the same constraint on integration time as is the Shack-Hartmann sensor, but multiple exposures of each laser pulse can, indeed must, be recorded. This leads to an improvement in the SNR of the derived wavefront phase.

Consider a Shack-Hartmann sensor used to measure N wavefront parameters (the local wavefront slopes). The sensor would use $N/2$ subapertures, and a detector with, optimally, $2N$ pixels. For the phase diversity sensor, to determine N parameters (now the pupil phases directly), at least two images are required, each with N illuminated pixels. (Here, "illuminated" means the noise in each of the pixels must be photon limited.) Again, $2N$ pixels are required. However, because both images can separately have the same integration time as the single image recorded by the Shack-Hartmann sensor, the phase diversity sensor has an advantage of a factor of two in total photon count. Generalizing the argument, if n_f images are recorded in the phase diversity sequence, an independent estimate of each phase value in the pupil can be obtained from each pair of images, so the expected advantage in SNR over the Shack-Hartmann sensor is roughly $\sqrt{n_f}$.

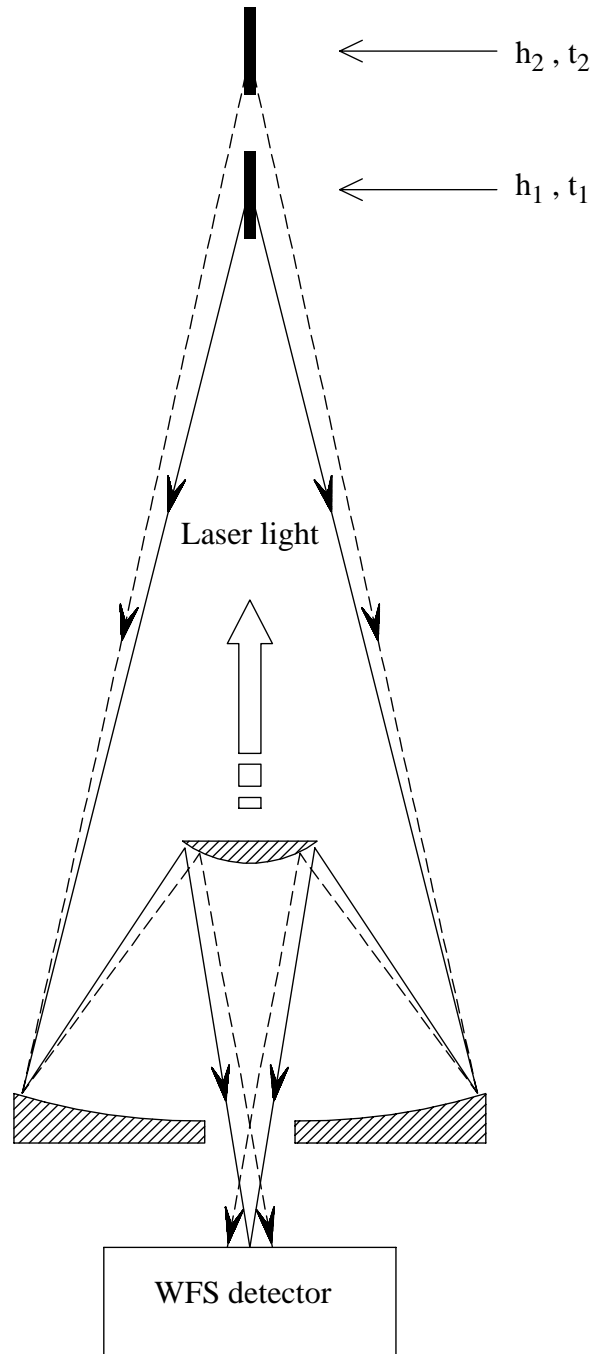


Figure 1. Geometry of the phase-diverse Rayleigh beacon wavefront sensor. A laser pulse fired into the atmosphere from behind the telescope's secondary mirror sends back Rayleigh scattered light to the telescope as it propagates. When the pulse passes through the height at which the detector is focused (h_1 at time t_1), a focused image is recorded. Some microseconds later at time t_2 , the pulse, now at height h_2 , sends back light which forms a defocused image on the wavefront sensor detector.

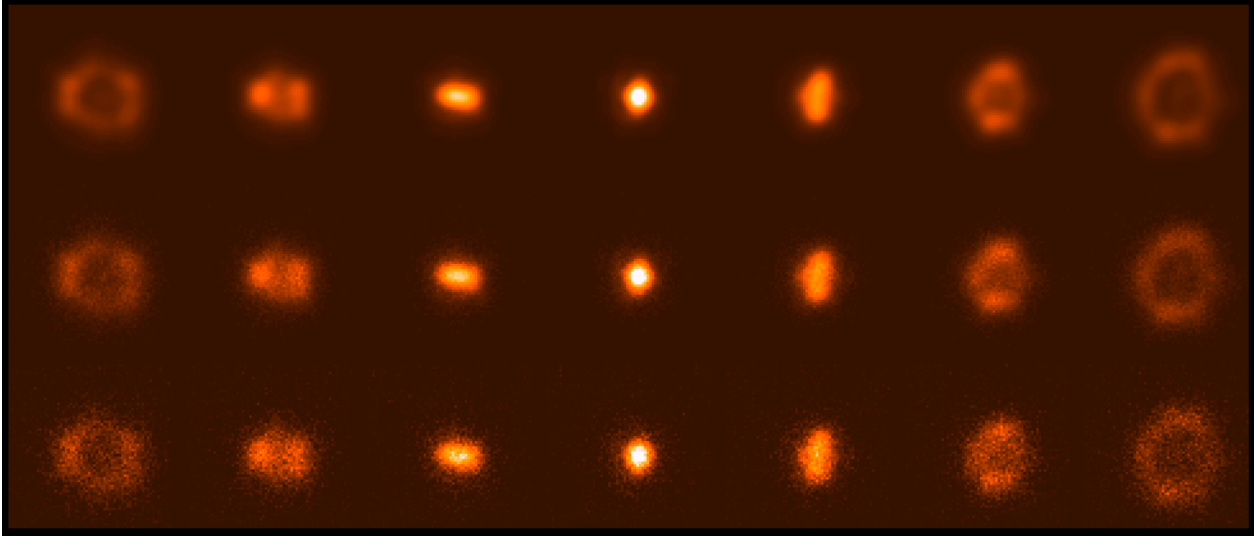


Figure 2. Simulated sequences of 7 frames showing a laser pulse as it passes through focus. At top is the noise-free case; center are the same images with Poisson noise equivalent to 50,000 photons per exposure, appropriate to a laser pulse of ~ 100 mJ; at bottom is the case with 10,000 photons per exposure.

4. SIMULATION OF WAVEFRONT SENSING

The frames of figure 2 contain multiply redundant information about the phase aberration accumulated by the laser beam in both the upward and downward paths. Since Rayleigh scattering does not preserve coherence in the laser beam, images of the beacon seen back at the telescope record the instantaneous point-spread function (PSF) of the atmosphere and telescope optics in the downgoing path, convolved with the PSF of the beam projector and the upgoing path. If the beam is projected through a small enough aperture that the only significant aberration in the upward path is tilt, then the phase recovered from the extra-focal images is a good measure of the pupil-plane distortion of the downgoing light.

We have modeled the case of a single beacon projected along the axis of a 6.5 m telescope. We take the average beacon height to be 20 km. Such an arrangement is not sufficient to give a good measurement of the phase aberration of starlight, because the uncertainty due to focal anisoplanatism would be very large. Nevertheless, one can investigate how well phase in the downgoing cone can be measured. In a multi-beacon setup, knowledge of the phase fronts in the overlapping cones swept out by all the beacons can be combined to give a tomographic view of the aberration.

The beacon was modeled as a 100 mJ pulse at 355 nm, typical output from a 50 W tripled YAG laser. The return flux from 20 km altitude was set to 120 photons/m² per mJ of laser energy per km of scattering path, derived from measurements by Thompson & Castle⁷ and Thompson⁸ with an excimer laser at Mt. Wilson. Including the expected photon efficiencies of the optics and detector (assumed combined value 0.4), the return flux through the aperture was taken to be 25,000 photons/ μ s.

Atmospheric turbulence was modeled as 3 discrete frozen layers propagating with different velocities at heights of 1, 5, and 10 km above the telescope. The combined seeing was equivalent to the median value observed at the site of the 6.5 m MMT ($r_0 = 10$ cm at 355 nm, 15 cm at 500 nm), with a mean height of 5500 m. Images were computed for 7 different heights of the beacon pulse, centered around 20 km with 300 m spacing, corresponding to a 2 μ s exposure time. To simulate the effect of the finite integration, 35 instantaneous atmospheric point-spread functions (PSFs) were computed at intervals of 400 ns, and then binned by 5 along the time axis. The atmospheric PSFs were convolved with the shape of the laser beam after propagation upward to 20 km through the same atmosphere. The images were computed on a 32×32 raster, simulating a detector with 0.16 arcsec pixels. Finally, photon noise was added at the level of 50,000 photons per frame. Two other cases with 10,000 and 25,000 photons per frame were also computed. Results are shown in figure 2.

The instantaneous PSF of the beacon at 20 km in this model was close to diffraction limited at 0.6 arcsec FWHM. Radial smearing of the speckle structure in the downgoing PSF was limited by the 2 μ s exposure time to 0.5 arcsec in the worst cases (at the edges of the maximally defocused images). Since these blurring effects add in quadrature, the integrated images are not substantially less sharp than an instantaneous snapshot.

Over the few microseconds required to record the entire sequence, evolution of the atmosphere is negligible. However, because the images in the sequence come from different heights, their paths through the atmosphere are not quite the same; the cone angle defined by the returning rays becomes more acute. Although this effect is not large for a telescope of 6.5 m diameter, it has been included in the model. It will become of greater significance when the technique is applied to very large telescopes of 30 m or larger.⁹

5. PHASE ESTIMATION FROM FOCAL-PLANE IMAGES

The approach taken in the estimation of pupil-plane phases from focal-plane image intensities is to model the images mathematically in terms of the desired phases. An error metric is then defined which measures the difference between the recorded image data and the images derived from the model by an assumed set of phase values. By differentiating the expression for the metric with respect to the phase values, one can determine the effect on the metric (and hence the quality of the reproduced images) of small variations in the phases. One then calculates a value for the metric given some assumed values of the phases, and changes the values iteratively until convergence is reached.

In the present case, we have assumed that the images are in the photon-limited noise regime. In this case, an error metric which provides the maximum likelihood phase estimate is given by:

$$\varepsilon = \sum_k \sum_x \hat{g}_k(x) - g_k(x) \ln \hat{g}_k(x) , \quad (1)$$

where $g_k(x)$ is the k th observed image and $\hat{g}_k(x)$ is the model of that image.

The model we have used is based on the laser beam profile $\gamma(x)$ at the exit pupil and the coherent point-spread functions $e(x)$ and $a_{k,l}(x)$ for the transmitted and received beams respectively:

$$\hat{g}_k(x) = \left[\gamma \otimes e \cdot e^* \otimes \sum_l w_l \cdot a_{k,l} \cdot a_{k,l}^* \right] , \quad (2)$$

where

$$e(x) = N^{-2} \sum_u P_T(u) \cdot \exp\left(i \left[(\psi \otimes \eta)_u - \frac{2\pi}{N}(x + \delta x) \cdot u \right]\right) , \quad (3)$$

$$a_{k,l}(x) = N^{-2} \sum_u P_R(u) \cdot \exp\left(i \left[(\psi \otimes \eta)_u + d_{k,l} \zeta(u) - \frac{2\pi}{N}(x + \delta x) \cdot u \right]\right) . \quad (4)$$

Here, \otimes denotes convolution, ψ_u are the phase variables to be estimated, $P_T(u)$ and $P_R(u)$ are the transmitting and receiving pupil amplitudes respectively, $\eta(u)$ is a smoothing kernel, δx is the offset of the image's center of mass (global tilt), $\zeta(u)$ is defocus phase diversity with amplitude $d_{k,l}$ and w_l is a weight associated with numerical integration of the 35 original frames down to seven.

The smoothing kernel has the effect both of reducing the number of independent degrees-of-freedom of the system and making the phase estimates resistant to "phase tears" (rapid changes in phase which are unphysical but which do not affect the incoherent point-spread-function estimate). It is chosen to smooth the phase over scales smaller than the Fried parameter r_0 at the wavelength of interest for science observations. Its value is given by

$$\begin{aligned} \eta(u) &= B \cdot \exp(-(r(u)/0.33r_0)^2) & r(u) \leq r_0 \\ &= 0 & r(u) > r_0 \end{aligned}$$

where $r(u)$ is the radial ordinate in the Fourier plane and B normalizes the kernel to unit volume.

The numerical implementation of the phase-diverse algorithm uses the derivatives of eq. (1) with respect to ψ_u to find both the phases and the image estimates $\hat{g}_k(x)$.

6. RESULTS

Global tilt is not measurable with this technique, for the same reason as for other schemes using laser beacons. The phases input to the numerical simulation therefore had tip and tilt explicitly removed. Distortion however is recoverable with high fidelity, as shown in figure 3. When the noise-free images are used, the phase estimate is almost indistinguishable from the true phase, as shown by the difference, which is nearly zero everywhere. The difference in fact is dominated by rounding error in the computer. The estimate derived from the images with 50,000 photons per frame is also extremely good. The residual phase error left from this more realistic case shows “blobbiness” on the scale of the smoothing kernel η .

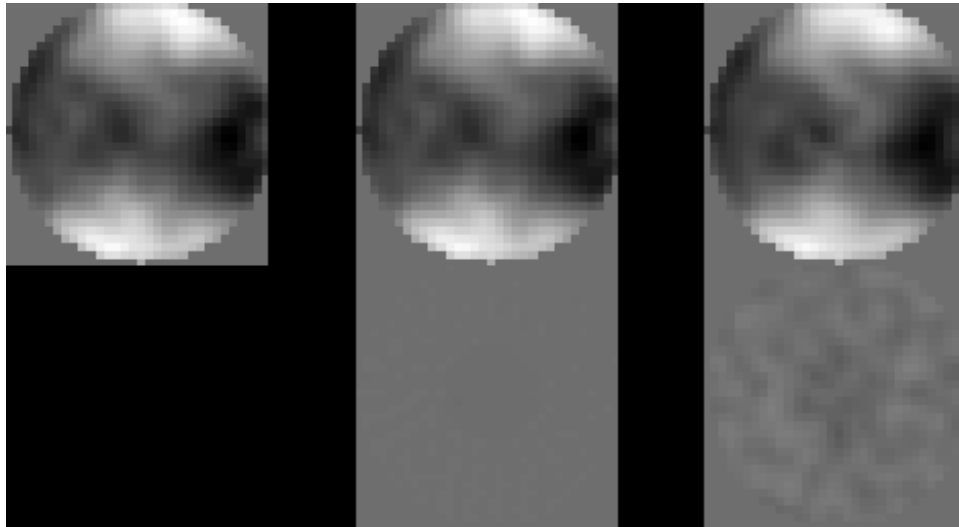


Figure 3. Results of the numerical simulation. At top left is the true phase accumulated by the beacon in its downward path from 20 km. In the center is the estimate obtained from the noise-free images of figure 2, and the difference between that estimate and the true phase, which is almost zero everywhere. At right is the phase estimate and the phase difference derived from the images with 50,000 photons per frame.

Figure 4 shows quantitatively the reduction in mean square phase error as a function of photon noise in the seven frames. For the canonical value of 50,000 photons, the reduction by two orders of magnitude would be sufficient to give a diffraction-limited image at 1 μm . This result was obtained after 10 iterations of the phase-diverse algorithm, which in practice would be rather slow. We have shown in separate experiments however that in a closed-loop system, the phase estimate from time-step n is an excellent starting assumption for the estimate of the phase at time $n+1$, and that only one iteration is required to update the phase estimate.

7. CONCLUSIONS

We have shown a new method for deriving wavefront phase estimates from Rayleigh laser guide stars. Because the technique takes advantage of multiple snapshots of each laser pulse per cycle of the adaptive optics loop, it has a fundamental advantage in photon count and hence SNR over other wavefront sensing methods with lasers. The technique will have particular application to very large telescopes where a single laser beacon, even at the high altitude of the sodium layer, will be unusable because of focus anisoplanatism. The method also naturally addresses the need for multiple guide stars to extend the isoplanatic patch with multi-conjugate adaptive optics.

Future work will see the addition of more physics to the simulations. In particular, we will add detector read noise, and characterize the phase in terms of a modal basis set. By solving for a limited number of modal amplitudes rather than very many phase values directly, the computational intensity of the problem can be greatly reduced.

We have recently begun bench-top experiments to simulate the technique with real light. Following that, we expect to construct a small testbed for initial measurements at a telescope, where a simultaneous Shack-Hartmann sensor will give ground-truth information. The hardware will rely on Pockels cells to provide the very fast gating for the cameras.

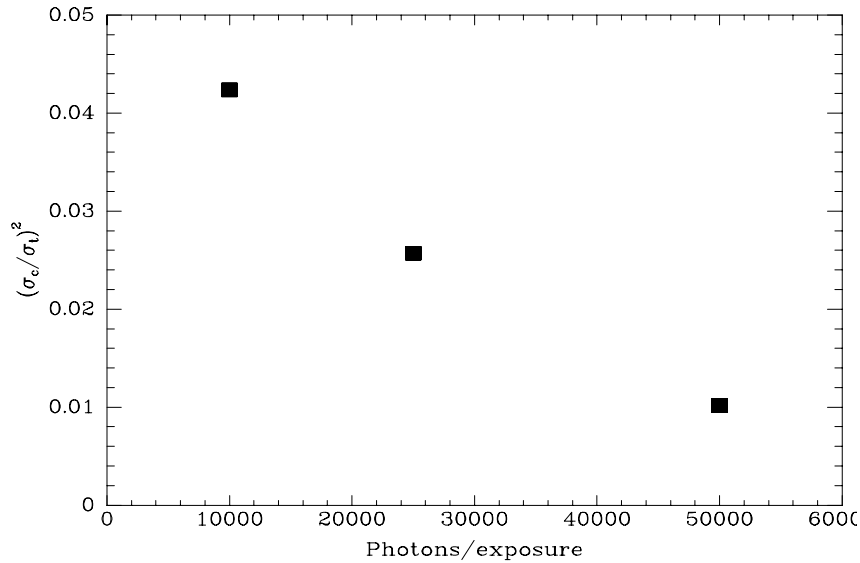


Figure 4. Degradation of the measured wavefront with photon noise. For the cases with 10,000, 25,000 and 50,000 photons per frame, we plot the ratio of the mean square residual phase error σ_c^2 to the mean square value σ_t^2 of the true phase.

ACKNOWLEDGEMENTS

This work has been supported by the Air Force Office of Scientific Research under grant number F49620-99-1-0285.

REFERENCES

1. J. Ge et al., *Adaptive Optical System Technologies* (Proc. SPIE), ed. D. Bonaccini & R. K. Tyson, **3353**, 242, 1998.
2. R. A. Gonsalves, *Opt. Eng.*, **21**, 829, 1982.
3. R. G. Paxman, T. J. Schulz, & J. R. Fienup, *JOSA A*, **9**, 1072, 1992.
4. M. Lloyd-Hart, et al., *ApJ*, **390**, L41, 1992.
5. M. Lloyd-Hart, et al., *ApJ*, **402**, L81, 1993.
6. R. Q. Fugate, *Adaptive Optical System Technologies* (Proc. SPIE), ed. D. Bonaccini & R. K. Tyson, **3353**, 22, 1998.
7. L. A. Thompson, & R. M. Castle, *Opt. Lett.*, **17**, 1485, 1992.
8. L. A. Thompson, *Adaptive Optics in Astronomy* (Proc. SPIE), ed. M. A. Ealey & F. Merkle, **2201**, 1074, 1994.
9. J. R. P. Angel, these proceedings.